Structure and Orientation of a Voltage-Sensor Toxin in Lipid Membranes

Hyun Ho Jung,[†△] Hoi Jong Jung,[†△] Mirela Milescu,[‡] Chul Won Lee,[§] Seungkyu Lee,[†] Ju Yeon Lee,[†] Young-Jae Eu,[†] Ha Hyung Kim,[¶] Kenton J. Swartz,[‡] and Jae Il Kim[†*]

[†]Department of Life Science, Gwangju Institute of Science and Technology, Gwangju, Korea; [‡]Molecular Physiology and Biophysics Section, Porter Neuroscience Research Center, National Institute of Neurological Disorders and Stroke, National Institutes of Health, Bethesda, Maryland; [§]Department of Molecular Biology and the Skaggs Institute of Chemical Biology, The Scripps Research Institute, La Jolla, California; and [¶]College of Pharmacy, Chung-Ang University, Seoul, Korea

ABSTRACT Amphipathic protein toxins from tarantula venom inhibit voltage-activated potassium (Kv) channels by binding to a critical helix-turn-helix motif termed the voltage sensor paddle. Although these toxins partition into membranes to bind the paddle motif, their structure and orientation within the membrane are unknown. We investigated the interaction of a tarantula toxin named SGTx with membranes using both fluorescence and NMR spectroscopy. Depth-dependent fluorescence-quenching experiments with brominated lipids suggest that Trp^{30} in SGTx is positioned ~9 Å from the center of the bilayer. NMR spectra reveal that the inhibitor cystine knot structure of the toxin does not radically change upon membrane partitioning. Transferred cross-saturation NMR experiments indicate that the toxin's hydrophobic protrusion contacts the hydrophobic core of the membrane, whereas most surrounding polar residues remain at interfacial regions of the bilayer. The inferred orientation of the toxin reveals a twofold symmetry in the arrangement of basic and hydrophobic residues, a feature that is conserved among tarantula toxins. These results have important implications for regions of the toxin involved in recognizing membranes and voltage-sensor paddles, and for the mechanisms by which tarantula toxins alter the activity of different types of ion channels.

INTRODUCTION

Voltage-activated ion channels open and close in response to changes in membrane voltage, a property that is fundamental to their roles in electrical and chemical signaling. These channels are comprised of two types of domains: a pore-forming domain constructed from the tetrameric arrangement of S5-S6 segments, and four voltage-sensing domains, each comprised of the S1–S4 segments (1). X-ray structures of the S1–S4 voltage-sensing domains in voltage-activated potassium (Kv) channels highlight a particularly interesting helix-turn-helix motif composed of the S3b helix and the charge-containing S4 helix (2–5). The paddle motif is the uniquely mobile region within voltage-sensing domains, and the motif moves in contact with the surrounding lipid membrane in response to changes in voltage (1,6–17).

A large number of protein toxins have been isolated from venomous organisms and shown to modify the gating mechanism in different types of voltage-activated ion channels by interacting with S1–S4 voltage-sensing domains. For example, hanatoxin from tarantula venom and the α- and β-scorpion toxins are thought to bind directly to the voltage-sensor paddle motifs in Kv channels or voltage-activated Na^+ (Nav) channels, with the S3b helix forming a particularly crucial area of the toxin receptors (12,15,18–24). Although the mechanisms by which these toxins modify channel gating are not yet fully understood, hanatoxin has been shown to inhibit Kv channels by stabilizing a resting/closed conformation of the voltage-sensor paddle (25,26), whereas the β-scorpion toxins facilitate opening of Nav channels by stabilizing a voltage sensor in an activated state (21). One particularly fascinating aspect of the mechanism by which voltage-sensor toxins work is that some appear to partition into the membrane and bind to the paddle motif at the protein-lipid interface. Hanatoxin and several related tarantula toxins, including VSTx, GsMTx, ProTx-II, SGTx, and GxTx-1E have been shown to partition into lipid membranes (13,17,26–31). The ability of these toxins to interact with membranes may arise from a common feature seen in their solution structures; one face of the toxin is highly amphipathic, containing a cluster of solvent-exposed hydrophobic residues that are surrounded by highly polar residues (29,32–34). In the case of SGTx (35), a Kv channel inhibitor whose structure and activity is very similar to hanatoxin (34), the amphipathic face of the toxin has been shown to be an important determinant of toxin activity (36). At present, however, little is known about how these toxins interact with membranes. How deep do they penetrate into the membrane? Does the toxin structure change upon partitioning from aqueous solution into the membrane? How are these toxins oriented with respect to the structure of the membrane? In this study, we utilize fluorescence and NMR spectroscopy to address these questions for SGTx, one of the better studied gating modifier toxins that can be readily produced using either solid-phase peptide synthesis or the recombinant method. In particular, we employ transferred cross-saturation (TCS) NMR methods (37–39) to identify the residues on SGTx that are in close proximity to the hydrophobic core of the membrane. Our results argue for a particular position and orientation of the toxin in the membrane, and uncover a twofold symmetry in the toxin

Submitted December 29, 2009, and accepted for publication April 20, 2010.

△Hyun Ho Jung and Hoi Jong Jung contributed equally to this work.

*Correspondence: jikim@gist.ac.kr

Editor: Francisco Bezanilla.

0006-3495/10/07/0638/9 $2.00

doi: 10.1016/j.bpj.2010.04.061

structure that may be crucial in positioning the toxin to bind voltage-sensor paddles.

MATERIALS AND METHODS

Synthesis of SGTx

SGTx was produced using solid-phase peptide synthesis and a recombinant expression system. Solid-phase peptide synthesis was conducted on an Applied Biosystems (Foster City, CA) model 433A peptide synthesizer. The synthetic SGTx was purified as described (34). SGTx was also expressed in *Escherichia coli* by using a bacterial ketosteroid isomerase (KSI) fusion protein system. In this system, SGTx is fused with the C-terminus of KSI, which contains Met at its N-terminus. The gene encoding SGTx as the KSI fusion protein was subcloned into pET31b using the *XhoI* restriction site. *E. coli* BL21 (DE3) cells were transformed with the expression construct and grown in either Luria Bertani media or M9 minimal media enriched with the desired stable isotope for NMR experiments. The expressed KSI-SGTx fusion protein was cleaved with CNBr to remove the N-terminal Met and separated by reverse-phase high-performance liquid chromatography. The amino acid sequence of SGTx (TCRYLFGGCKTTADCCKHLACRSDGKYCA WDGTF) was confirmed by a time-of-flight mass spectroscopy measurement. Because all of the Cys residues in SGTx were fully reduced after purification, SGTx was oxidized into the native fold as previously described (34).

Preparation of lipid vesicles

Phospholipids were dried from a chloroform solution under a nitrogen stream and the residual solvent was removed under vacuum. The dried lipid film was rehydrated in 10 mM HEPES, 1 mM EDTA, pH 7.0, for fluorescence spectroscopy or 10 mM phosphate buffer, pH 5.8, for NMR spectroscopy. The resulting dispersions were extruded through polycarbonate filters with a 100-nm pore size (Millipore, Bedford, MA) to form large unilamellar vesicles (LUVs) for fluorescence spectroscopy or tip-sonicated on ice to form small unilamellar vesicles (SUVs) for NMR spectroscopy.

Depth-dependent quenching of tryptophan fluorescence by brominated phosphatidylcholines

All fluorescence measurements were performed in quartz cuvettes with a 1-cm path length. For control experiments, LUVs composed of 1:1 molar ratios of 1-palmitoyl-2-oleoyl-*sn*-glycero-3-(Phospho-*rac*-(1-glycerol)) (POPG) and 1-palmitoyl-2-oleoyl-*sn*-glycero-3-phosphocholine (POPC) were added to a solution of SGTx (3 μM final concentration), maintained at 298 K with continuous stirring in a total volume of 2 ml. For quenching experiments with brominated lipids, LUVs contained a 1:1 molar ratio of POPG and POPC 6,7-, 9,10-, or 11,12-1-palmitoyl-2-stearoyl(dibromo)-*sn*-glycero-3-phosphocholine (diBr; Avanti Polar Lipids, Alabaster, AL). Fluorescence spectra (averaging three spectra) were recorded between 300 and 400 nm (5-nm bandpass, 0° polarizer) using an excitation wavelength of 270 nm (5-nm bandpass, 90° polarizer) (FluoroMax 3 spectrofluorometer, SPEX, Metuchen, NJ), corrected for vesicle scattering (40) and normalized to the zero lipid fluorescence intensity. The quenching of tryptophan fluorescence by brominated lipids was used to calculate the average insertion depth of the tryptophan residue (h_m) using both distribution analysis (DA) (41,42) and the parallax method (PM) (43,44). h_m was calculated based on the best fit of the following equations to the data: for DA calculations, $\ln(F_o/F_h) = S/(\sqrt{2})\exp(-(h - h_m)^2/2$; and for the PM method, $\ln(F_o/F_h) = Cf[R_c^2 - (h - h_m)^2]$ when $h - h_m < R_c$, and $\ln(F_o/F_h) = 0$ when $h - h_m \geq R_c$. F and F_0 are the fluorescence intensities in the absence and presence of diBr quenchers determined by integration of emission spectra between 300 and 450 nm, h is the depth of the quencher based on x-ray diffraction measurements, C is the quencher concentration, S is area, σ is dispersion, R_c is the radius of quenching, and f is the fraction of the quencher in the vicinity of the tryptophan residue. We also analyzed the quenching data allowing for distribution of the toxin in both leaflets and obtained similar results.

NMR spectroscopy

All experiments were performed at 288 K on an Avance 600 spectrometer (Bruker, Billerica, MA). For conformational analysis of SGTx in the presence of membranes, uniformly ^{15}N-labeled SGTx and SUVs at a concentration of 0.4 mM with POPC were dissolved in 10 mM phosphate buffer, pH 5.8, containing 90% H_2O and 10% D_2O, and used to record a 3D ^{15}N-TOCSY heteronuclear single quantum coherence (HSQC) spectrum with 80 ms mixing time and 3D ^{15}N nuclear Overhauser effect spectroscopy (NOESY)-HSQC spectra with 80, 150, and 250 ms mixing time. Sodium 3-(trimethylsilyl)-2,2,3,3-tetradeuteropropionate (TSP) was used for reference of ^{1}H chemical shift at 0 ppm, utilized for calculation of the ^{15}N chemical shift. Also, the chemical shift perturbations of SGTx in the presence of vesicles with different concentrations were achieved by 2D ^{1}H-^{15}N HSQC spectra, and were calculated according to the equation $\delta = [(\Delta H_N)^2 + (\Delta N \times 0.17)^2]^{1/2}$. The chemical shifts were classified as follows: no chemical shift change, $\delta = 0$–0.05; small chemical shift change, $\delta = 0.05$–0.10 (45,46). ^{15}N relaxation measurements were performed at nine relaxation delays ranging from 50 to 900 ms using uniformly ^{15}N-labeled SGTx with and without vesicles. The exponential curve fitting of T1 was conducted by SPARKY (47). TCS experiments were carried out as previously described (37–39). Uniformly ^{2}H-^{15}N-labeled SGTx and the SUVs were prepared at the same concentration, buffer, and pH as uniformly ^{15}N-labeled SGTx, containing 20% H_2O and 80% D_2O. The pulse scheme and the decoupling pulse used for the experiment were the same as described previously (37). We selectively saturated the vesicles by irradiating resonances from the phospholipid alkyl chains, using the WURST-2 broadband decoupling scheme. The saturation frequency was set at 0.9 ppm, and the maximum radio frequency amplitude was set to 0.17 kHz. The saturation time was set at 1.1 s, and the delay was set at 2.0 s. Because the saturation scheme is highly selective for the aliphatic proton region of phospholipid vesicles, irradiation of the phospholipid vesicle-SGTx complex affects neither the intensities of the SGTx amide protons nor the water resonance. All spectra were processed by XWIN-NMR, and the SPARKY software assisted data analysis (47).

RESULTS

Membrane partitioning of SGTx

SGTx contains a single tryptophan residue (Trp^{30}) on the hydrophobic surface of the toxin, and aqueous solutions of the toxin exhibit fluorescence emission after excitation at 270 nm that are typical for a tryptophan residue exposed to a polar environment (Fig. 1 *a*, *black line*). When lipid vesicles containing a 1:1 mixture of POPG and POPC are mixed with the toxin, the emissions spectrum shifts toward lower wavelengths (blue shift), as expected for movement of tryptophan from a polar to a hydrophobic environment (Fig. 1 *a*, *gray line*). To provide an estimate of the depth to which SGTx partitions into membranes, we examined quenching of Trp fluorescence by bromine atoms attached at different positions along the hydrocarbon chain of POPC (41,42). The fractional quenching of tryptophan fluorescence by bromine atoms is most pronounced when the quencher is attached near the middle of the phospholipid hydrocarbon chain (9,10-diBr) (Fig. 1). Analysis of the quenching profile for the three different brominated lipids (43,44) suggests that Trp^{30} is positioned ~9 Å from the center of the bilayer.

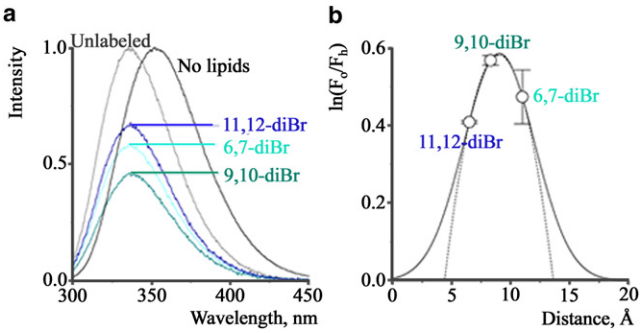

FIGURE 1 Depth-dependent quenching of tryptophan fluorescence by brominated phosphatidylcholines. (*a*) Fluorescence emission spectra for SGTx in the absence and presence of lipid vesicles containing unlabeled or brominated (diBr) lipids. (*b*) Analysis of the depth-dependent quenching profiles for SGTx. Fractional quenching (F_0/F_h) by brominated lipids plotted as a function of the average distance of bromine atoms from the center of the bilayer. Solid lines correspond to DA, where $h_m = 9$ Å, $S = 0.86$, and $\sigma = 0.33$; dashed lines correspond to PM analysis, where $h_m = 9$ Å, $f = 0.04$, and $R_c = 4.6$ Å. Data points are the mean ± SE ($n = 3$).

Structure of SGTx in the presence of membranes

The structure of SGTx in aqueous solution was previously solved by our group using NMR (34). The molecular structure consists of a triple-stranded antiparallel β-sheet and four chain reversals, indicating that the backbone structure of the toxin is generally well defined. To examine whether the structure of the toxin is altered upon partitioning into zwitterionic (POPC) membrane, a mimic of mammalian membrane, we looked for chemical-shift perturbations using ^{1}H-^{15}N HSQC spectra (Fig. 2 *b*). Chemical-shift perturbations are often used as a sensitive probe for chemical environment or conformational changes observed at the interface of intermolecular interaction (48,49). As shown in Fig. 2 *b*, although SGTx contains 34 residues, significant chemical-shift perturbations (>0.035 ppm) were observed for only five residues (Leu^5, His^{18}, Trp^{30}, Asp^{31}, and Phe^{34}), suggesting that the entire structure of the toxin does not change dramatically. Considering that the partitioning of SGTx into POPC membranes is weak, with an estimated mole fraction partition coefficient (K_x) between 10^4 and 10^5 (Fig. S1 in the Supporting Material), it seems likely that there is a rapid chemical exchange between bound and free SGTxs, leading to coalescence of the NMR signals into averaged signals at chemical shifts between those of the bound and the free state. In the solution structure, Leu^5 lies in a type II β-turn (Tyr^4–Gly^7), which is surrounded by several hydrophobic residues, and His^{18} and Trp^{30} are located at a type IV β-turn (Cys^{16}–Leu^{19}) and a β-strand III (Tyr^{27}–Trp^{30}), respectively. It is of interesting that two residues, Asp^{31} and Phe^{34}, lie outside the inhibitor cystine knot region within a C-terminal segment (Asp^{31}–Phe^{34}) that is highly flexible in aqueous solution. Although these five residues are sprinkled through the primary sequence and the secondary structural elements of the toxin, they neatly cluster in the three-dimensional structure of the toxin near the C-terminal region. Next, we carefully compared the NOE patterns on NOE spectra obtained in the absence and presence of membranes. If the structure of SGTx changes upon partitioning into membranes, new crosspeaks for the membrane-bound toxin would be expected in NOESY spectra. Unfortunately, however, no new crosspeaks were observed. Taken together, these results suggest that the observed chemical-shift perturbations probably result from local environmental changes that are limited to a defined portion of the toxin structure.

Membrane binding mode of SGTx

To constrain the position and orientation of SGTx in the membrane, we identified those residues in close proximity to the hydrophobic core of the membrane using TCS NMR experiments (37–39). We used deuterated SGTx for these TCS measurements so that irradiation of the complex with a frequency corresponding to the proton resonances of the phospholipid alkyl chains would only directly affect lipid molecules. The irradiation causes the effective saturation of all phospholipid resonances due to spin diffusion. The saturation in the phospholipids is not limited to the membrane vesicles but is transferred to SGTx residues at the protein-lipid interface through the cross-saturation phenomena. TCS experiments are applicable to weak molecular interactions where the dissociation rate should be $>0.1\ s^{-1}$ to effectively transfer cross saturation to the free state of a ligand according to the complete relaxation and conformational exchange matrix (CORCEMA) theory (37,50). The partitioning of SGTx into mixed POPC/POPG vesicles is probably too strong ($K_x = 10^6$; Fig. S1) (13) to be suitable for TCS experiments, and thus we only examined the weaker interaction between SGTx and POPC membranes, mimicking the interaction between SGTx and mammalian membranes.

Peak intensities of the amide groups of free SGTx on ^{1}H-^{15}N HSQC spectra without and with irradiation are shown in Fig. 3 *a*. The irradiation applied to the NMR sample results in selective intensity losses for the free SGTx resonances (Fig. 3 *b*). Based on the spectra with and without irradiation, we calculated the reduction of peak intensities as a signal intensity ratio (Fig. 3 *c*). The greatest reductions in peak intensity are observed for Leu^5, the side chain of Trp^{30}, and Asp^{31}, which exhibit signal intensity ratios of <0.5, followed by Phe^6 and Gly^7, which exhibit ratios of 0.5–0.6. Substantial reductions are also observed for Tyr^4, Cys^{16}, Leu^{19}, Ala^{20}, Tyr^{27}, Cys^{28}, Ala^{29}, and Trp^{30}, with ratios of 0.6–0.7. Several other residues, such as Thr^{11} (30%), Asp^{14} (27%), Lys^{17} (29%), His^{18} (23%), G^{25} (32%), Lys^{26} (35%), and Phe^{34} (25%), are not considered from an estimation in peak intensity, because all of them exhibit T1 relaxation times that are reduced by >20% after addition of lipid vesicles, reflecting an occurrence of line broadening of peptide resonance due to membrane partitioning. It is interesting to note that the residues affected by irradiation of the membrane are distributed on a contiguous surface of SGTx (Fig. 4 *a*). Previous TCS

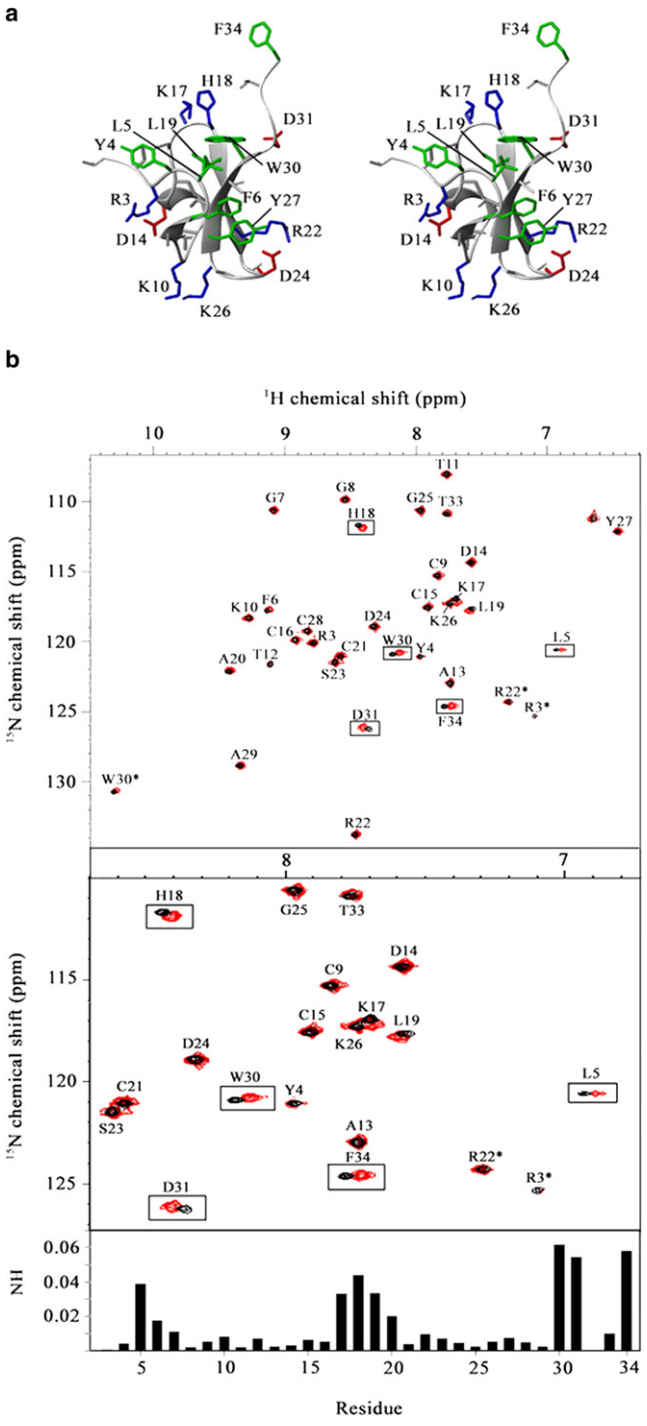

FIGURE 2 Structure of SGTx in the absence and presence of membranes. (*a*) Stereo pairs of the SGTx solution structure (Protein Data Bank (PDB) accession number, 1LA4). The side chains of hydrophobic, basic, and acidic residues are green, blue, and red, respectively. The structure topology of the β-sheet was identified by MOLMOL. (*b*) Chemical shift changes on ^{1}H-^{15}N HSQC spectra of 0.4 mM ^{15}N-labeled SGTx without POPC vesicles (*black*) and with 0.4 mM vesicles (*red*), indicating a peptide/lipid molar ratio of 1:1 in 90% H_2O and 10% D_2O. The assignments are indicated with the one-letter amino acid code and residue number. Residues showing absolute values of chemical-shift difference (δ) of >0.035 ppm (L5, H18, W30, D31, and F34) are boxed. Calculation of the chemical-shift change is detailed in Methods. The bar graph below the figure gives a summary of the chemical shift changes of SGTx in the presence of vesicles.

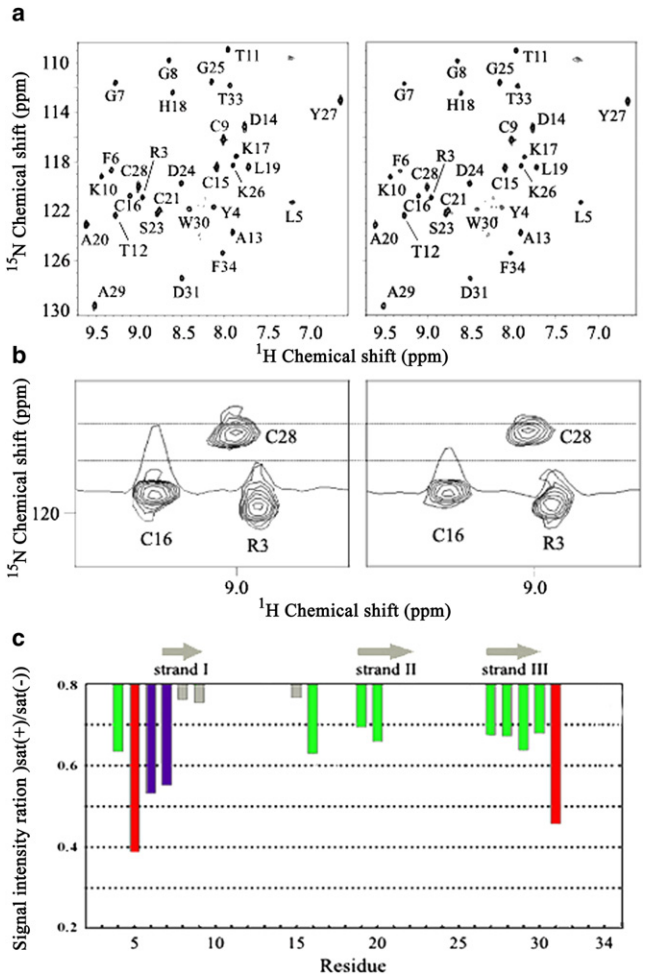

FIGURE 3 Transferred cross saturation between lipid and SGTx. (*a*) A ^{1}H-^{15}N HSQC spectrum of the SGTx in the presence of POPC vesicles without (*left*) and with (*right*) irradiation. (*b*) Cross sections and portions of a ^{1}H-^{15}N HSQC spectrum observed for labeled SGTx in the presence of nonlabeled POPC vesicles without (*left*) and with (*right*) irradiation. (*c*) Signal intensity ratios in the TCS experiments. Color scheme for signal intensity ratios: *red*, >0.5, *purple*, 0.5–0.6, *green*, 0.6–0.7, and *gray*, 0.7–0.8. The secondary structure of SGTx is represented by arrows for β-strands in the plot.

experiments suggest that efficient transfer (signal intensity ratios of ~0.5) occurs over molecular interface distances <7 Å and that ratios >0.8 represent transfer to residues not located at the molecular interface (37). Thus, we conclude that the surface of the toxin containing the hydrophobic protrusion (Fig. 4 *a*) dips into the hydrophobic core of the membrane. One polar residue, Asp^{31}, also contacts the hydrophobic core of the membrane. In contrast, most of the polar residues surrounding the hydrophobic surface, including Arg^3, Lys^{10}, Asp^{24}, and Arg^{22}, exhibit little or no reduction in peak intensity in TCS experiments, suggesting that they

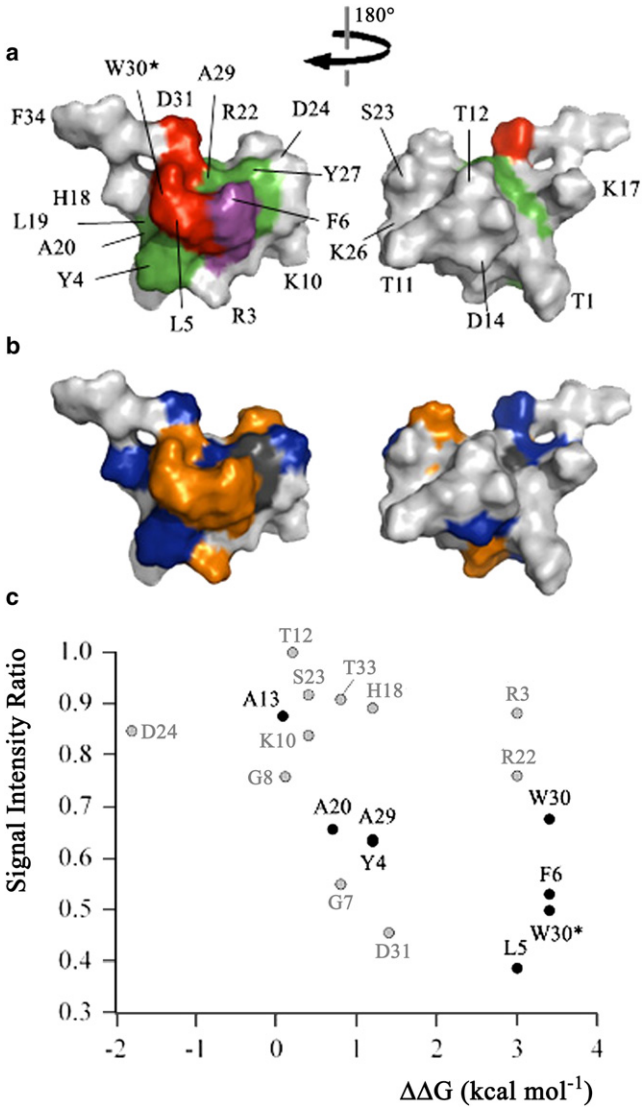

FIGURE 4 Comparison of TCS experiments with mutational analysis. (*a*) Mapping of residues in SGTx affected in TCS experiments. Color scheme for signal intensity ratios: *red*, <0.5, *purple*, 0.5–0.6, and *green*, 0.6–0.7. For Trp^{30}, the NH of the backbone is green, but the NH of the side chain is red (signal intensity ratio <0.5). (*b*) Mapping of interaction between SGTx and Kv2.1 channels resulting from mutations in SGTx. Mutants that display weaker binding affinity are colored light gray if |ΔΔG| values are <1 kcal mol^{-1}, blue if |ΔΔG| values are 1–1.5 kcal mol^{-1}, and orange if |ΔΔG| values are >1.5 kcal mol^{-1}. Unstudied residues (Leu^{19}, Tyr^{29}, and Cys^{6}) are colored dark gray. (*c*) Plot of perturbation energy (ΔΔG) from mutational analysis versus signal intensity ratio from TCS analysis. Hydrophobic residues are shown in black and all others in gray.

are positioned outside of the hydrophobic core of the membrane.

Comparison with mutational analysis

Previous alanine scanning mutagenesis of SGTx identifies an active surface where mutations have pronounced effects on the concentration-dependence for toxin occupancy of the channel, and a tolerant face where mutations have little if any effect (36). These mutagenesis results are interesting in the context of the TCS results presented here, because both highlight the same face of the toxin (Fig. 4, *a* and *b*). This relationship suggests that the active face of the toxin dips into the membrane, consistent with the notion that the toxin's receptor within the voltage sensor is actually positioned within the membrane. If one considers the relationship between signal intensity ratio in the TCS experiments and perturbations in toxin-binding free energy in scanning mutagenesis experiments (ΔΔG; Fig. 4 *c*), there are roughly two groups of toxin residues. Residues in the first group exhibit weak perturbations (ΔΔG <~1 kcal/mol) when mutated to Ala, whereas those in the second group exhibit more pronounced perturbations in toxin affinity (ΔΔG >3 kcal mol^{-1}). It is important to note that there is no obvious correlation between signal intensity ratio and perturbation energy, even if only hydrophobic residues are considered, arguing that the perturbation in toxin activity does not simply reflect perturbations in toxin partitioning. We suspect that residues in the second group (e.g., R3, L5, F6, R22, and W30) play key roles in the protein-protein interaction between the toxin and the voltage-sensor paddle. Other work suggests that the interaction between toxin and voltage sensor involves intimate interactions with lipids (17), which is consistent with our results, where residues such as L5, F6, and W30 interact intimately with lipids (low signal intensity ratio) and mutations dramatically weaken toxin affinity.

DISCUSSION

The immediate objective of this study is to constrain the structure, position, and orientation of a voltage-sensor toxin in the lipid membrane. The comparison of HSQC spectra for SGTx in the absence and presence of POPC membranes indicates that the structure of the toxin does not exhibit substantial alterations with membrane partitioning and an occurrence of a rapid chemical exchange between bound and free SGTxs. Several residues exhibit significant chemical shift perturbations, most likely reflecting changes in their environment as the toxin moves between aqueous and membrane phases.

The TCS experiments identify one group of residues positioned near or within the hydrophobic phase of the membrane (Tyr^{4}, Leu^{5}, Phe^{6}, Gly^{7}, Cys^{16}, Leu^{19}, Ala^{20}, Tyr^{27}, Cys^{28}, Ala^{29}, Trp^{30}, and Asp^{31}) and another group positioned outside the hydrophobic phase (Arg^{3}, Gly^{8}, Cys^{9}, Lys^{10}, Thr^{12}, Ala^{13}, Cys^{15}, Cys^{21}, Arg^{22}, Ser^{23}, Asp^{24}, and Thr^{33}). Together, these constraints are most consistent with positioning of the toxin superficially within the membrane such that the hydrophobic protrusion dips into the hydrophobic phase of the membrane leaving the majority of polar residues within the polar headgroup layer of the membrane (Fig. 5 *a*). This positioning of the toxin based on TCS results is consistent with the depth-dependent

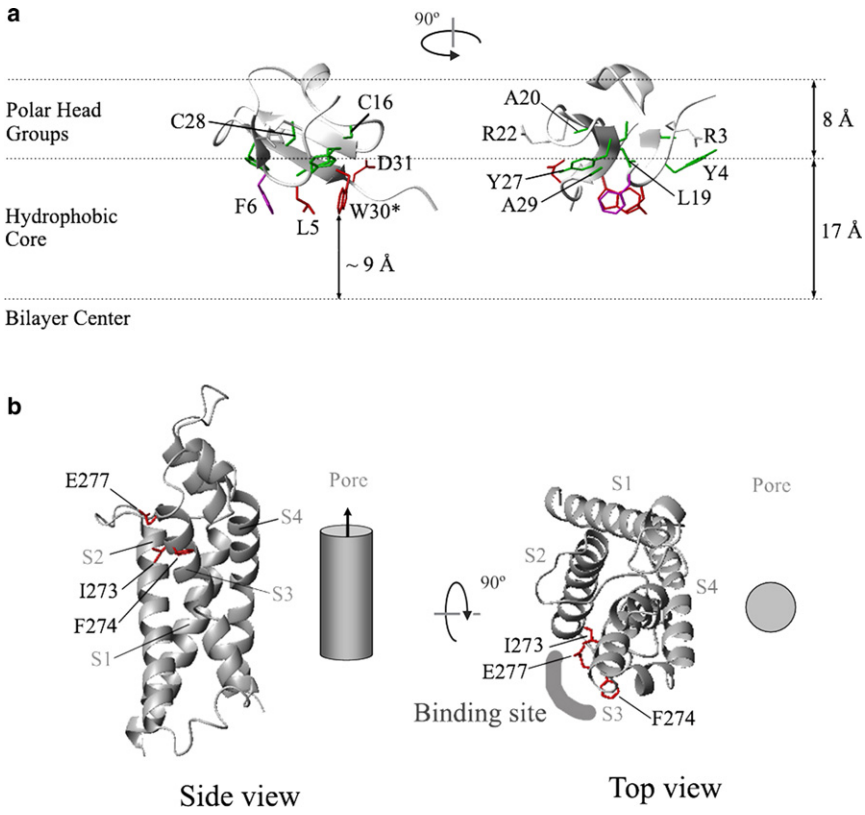

FIGURE 5 Orientation of SGTx interaction with membranes. (*a*) Position and orientation of SGTx in the lipid membrane as suggested by depth-dependent tryptophan quenching and TCS experiments. The SGTx structure is represented as an energy-minimized structure among 20 conformers. Residues are colored as in Fig. 2 *a*. Dashed lines are approximate demarcations to illustrate the hydrophobic core and polar headgroup regions for one leaflet of the membrane. (*b*) Side and top views of the voltage-sensing domain of a paddle-chimera channel, which inserted its S3b-S4 region of Kv2.1 into a Kv1.2 channel (PDB accession number, 2R9R), are represented in juxtaposition with the pore of the ion channel. Side chains of residues that are important for SGTx binding to the voltage sensor are colored red and labeled using numbering for Kv2.1.

fluorescence-quenching experiments, which position Trp^{30} ~9 Å from the center of the bilayer. Our observations are further supported by results of atomistic molecular dynamics simulations, which suggest that SGTx prefers to be located close to the membrane/water interface of the lipid bilayer (51). The overall picture is one in which the toxin position is tilted with respect to the membrane plane, rather than flat, with the C-terminus positioned deeper in the membrane than residues on the opposite end of the toxin (Fig. 5 *a*).

Implications for positioning of the voltage-sensor paddle

Tarantula toxins interact with the S3b and S4 helices of the voltage-sensor paddle of Kv channels (12,15,19,20,22,24,26), and toxins like SGTx inhibit opening by stabilizing a closed state (25,26). The position of SGTx as determined from TCS experiments would suggest that movements of the paddle motif are likely to be confined to the outer half of the bilayer, as previously inferred from positioning of the toxin based on fluorescence-quenching experiments (26). A more refined picture of how the paddle motif moves during voltage sensing would require the identification of specific side-chain interactions between toxin and paddle, and a better understanding of whether toxin-membrane interactions change when the toxin binds to the paddle motif. However, consideration of our TCS results together with previous mutagenesis results and the x-ray structure of the Kv1.2/2.1 chimera (2) suggest that the depth of the S3b helix within the membrane is relatively stable as the voltage sensors move. In Kv2.1, Phe^{274} is a particularly sensitive hydrophobic residue within the S3b helix, where mutations weaken toxin affinity by as much as 500-fold (22,24). In mutational analyses of SGTx (36), residues in the hydrophobic protrusion (e.g., Trp^{30}, Leu^{5}, and Phe^{6}) are the most likely candidates for making hydrophobic interactions with Phe^{274}. The TCS results presented here suggest that these hydrophobic residues would interact with Phe^{274} within the hydrophobic core of the membrane (Figs. 3 *c*, 4 *a*, and 5 *a*), which could help to explain the recent observation that the magnitude of perturbations in toxin affinity observed for mutations at Phe^{274} are dependent on lipid species (17). Another important residue in the S3b helix is Glu^{277}, a position where the substitution of basic residues is the most disruptive, weakening toxin affinity by as much as 125-fold (22,24). One possibility is that Glu^{277} forms a salt bridge with a basic residue on the toxin. Of the five basic residues on SGTx, mutations of only two (Arg^{3} and Arg^{22}) have a large enough effect to be candidates for interacting with Glu^{277} (36) (Fig. 4, *b* and *c*). It is interesting that in the TCS experiments, both Arg^{3} and Arg^{22} show relatively weak attenuation, suggesting that they are positioned within the polar headgroup region of the membrane (Fig. 5 *a*). Taken together, these constraints for F274 and E277 would suggest that the S3b helix straddles the boundary between the hydrophobic and polar headgroup regions of the bilayer

when the toxin is bound to the channel in a closed state. The x-ray structure of the Kv1.2/2.1 chimera shows a similar position of the S3b helix in the open state (2), suggesting that the depth of this helix does not dramatically change during gating, consistent with accessibility studies (52–54). If the S4 helix translates ~15 Å into the membrane to close the channel, as suggested by some studies (6,7), the interface between S3b and S4 helices seen in crystal structures would need to undergo significant rearrangement.

Symmetry in the tarantula toxin structure

The orientation of SGTx within a lipid membrane inferred from our TCS results (Fig. 5 *a*) reveals an approximate twofold symmetry in the structures of tarantula toxins that is most apparent when mapping hydrophobic and positively charged residues onto their structures (Fig. 6). The axis of symmetry lies roughly on a ridge running along the hydrophobic surface of the toxins that is comprised of Phe^{6}, Leu^{5}, and Trp^{30} in SGTx (and HaTx), Trp^{27}, Val^{29}, and Leu^{30} in VSTx, and Leu^{29}, Trp^{6}, and Phe^{5} in GsMTx. On either side of this ridge are paired residues that occupy similar positions: Lys^{26}-Arg^{3}, Tyr^{27}-Tyr^{4}, and Arg^{22}-Lys^{17} in the case of SGTx (and HaTx); Lys^{26}-Lys^{4}, Trp^{25}-Phe^{5}, and Arg^{24}-Lys^{17} in VSTx; and Lys^{28}-Lys^{8}, Lys^{25}-Lys^{15}, Phe^{27}-Trp^{7}, and Leu^{26}-Leu^{3} in GsMTx. Although the rationale for this symmetry is unclear, it is a conserved feature of tarantula toxins that interact with voltage sensors in Kv channels, including SGTx, hanatoxin, and VSTx (Fig. 6, *a–c*). Perhaps this symmetry allows these toxins to adopt a position and orientation that is necessary for forming a complex with the voltage-sensor paddle motif. It is particularly intriguing that this symmetry is also evident in the structure of GsMTx, a tarantula toxin that inhibits native stretch-activated cation (SAC) channels in astrocytes and heart cells (Fig. 6 *d*) (28,55,56). It is noteworthy that the D-enantiomer of this toxin is capable of inhibiting SAC channel activity, an observation that argues for an indirect toxin mechanism involving a perturbation of the bilayer mechanics rather than a direct protein-protein interaction (28). However, another possibility is that the symmetry observed here enables different residues in the D and L

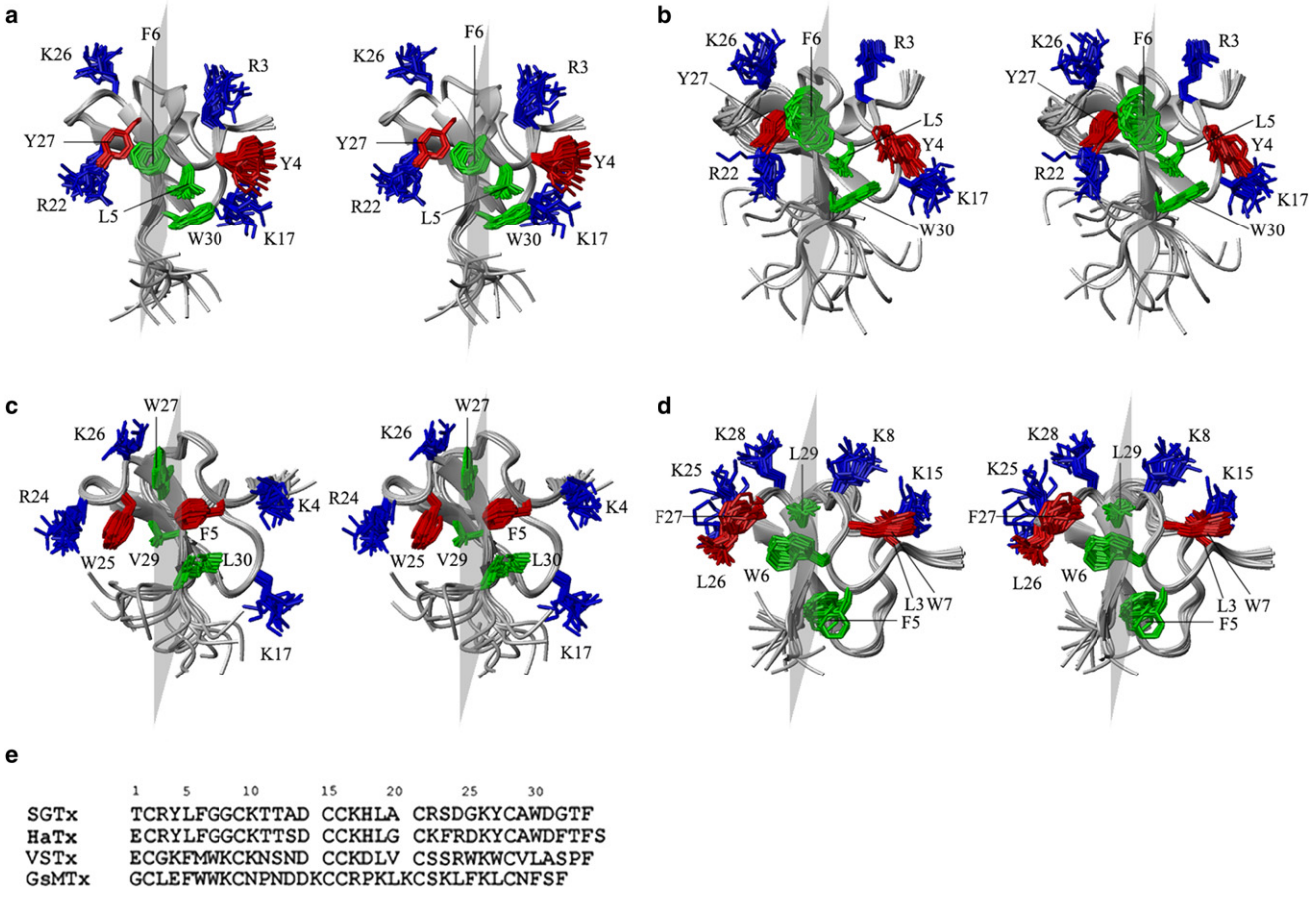

FIGURE 6 Approximate twofold symmetry in the distribution of hydrophobic and charged residues in tarantula toxins. (*a*) SGTx (PDB accession number, 1LA4). (*b*) hanatoxin (*HaTx*) (PDB 1D1H). (*c*) VSTx (1S6X). (*d*) GsMTx (1LU8). Structures are represented as bundles of 20 superimposed conformers. All toxins are shown as stereo pairs. Hydrophobic residues near the twofold axis are colored green, lateral hydrophobic residues are colored red, and lateral basic residues are colored blue. (*e*) Sequence alignment for toxins in *a–d*.

enantiomers to take part in crucial side-chain interactions at a protein-protein interface between the toxin and channel. Such a scenario seems reasonable when one considers that the protein-protein interaction occurs within the membrane and likely involves intimate interactions with specific lipids (17), giving the interface a somewhat pliable or flexible character. This idea might help to explain why many related tarantula toxins exhibit similar membrane partitioning, yet in some instances have different affinities for inhibition of SAC channels and in others are inactive altogether (55). For example, hanatoxin partitions with a K_x that is similar to GsMTx (13,26,28), yet this toxin does not inhibit SAC channels (55). Although the molecular identity of the SAC channel that GsMTx inhibits is unknown, we propose that it may be related to the voltage-activated ion channels that harbor voltage sensor-paddle motifs. The common structural symmetry that is found on the surface of voltage-sensor toxins may be helpful in designing therapeutic agents that target the paddle motif in voltage-activated ion channels.

SUPPORTING MATERIAL

A figure is available at http://www.biophysj.org/biophysj/supplemental/S0006-3495(10)00559-X.

This study was supported by grants from the Brain Research Center of the 21st Century Frontier Research Program (M103KV010006-06K2201-00610), the BioImaging Research Center at the Gwangju Institute of Science and Technology, the Korea Healthcare technology R & D Project, Ministry of Health and Welfare, Republic of Korea (A080712), and the Intramural Research Program within the National Institute of Neurological Disorders and Stroke, National Institutes of Health, Bethesda, MD.

REFERENCES

1. Swartz, K. J. 2008. Sensing voltage across lipid membranes. *Nature*. 456:891–897.
2. Long, S. B., X. Tao, …, R. MacKinnon. 2007. Atomic structure of a voltage-dependent K^+ channel in a lipid membrane-like environment. *Nature*. 450:376–382.
3. Long, S. B., E. B. Campbell, and R. Mackinnon. 2005. Crystal structure of a mammalian voltage-dependent *Shaker* family K^+ channel. *Science*. 309:897–903.
4. Lee, S. Y., A. Lee, …, R. Mackinnon. 2005. Structure of the KvAP voltage-dependent K^+ channel and its dependence on the lipid membrane. *Proc. Natl. Acad. Sci. USA*. 102:15441–15446.
5. Jiang, Y., A. Lee, …, R. MacKinnon. 2003. X-ray structure of a voltage-dependent K^+ channel. *Nature*. 423:33–41.
6. Ruta, V., J. Chen, and R. MacKinnon. 2005. Calibrated measurement of gating-charge arginine displacement in the KvAP voltage-dependent K^+ channel. *Cell*. 123:463–475.
7. Jiang, Y., V. Ruta, …, R. MacKinnon. 2003. The principle of gating charge movement in a voltage-dependent K^+ channel. *Nature*. 423:42–48.
8. Cuello, L. G., D. M. Cortes, and E. Perozo. 2004. Molecular architecture of the KvAP voltage-dependent K^+ channel in a lipid bilayer. *Science*. 306:491–495.
9. Chakrapani, S., L. G. Cuello, …, E. Perozo. 2008. Structural dynamics of an isolated voltage-sensor domain in a lipid bilayer. *Structure*. 16:398–409.
10. Schmidt, D., Q. X. Jiang, and R. MacKinnon. 2006. Phospholipids and the origin of cationic gating charges in voltage sensors. *Nature*. 444:775–779.
11. Ramu, Y., Y. Xu, and Z. Lu. 2006. Enzymatic activation of voltage-gated potassium channels. *Nature*. 442:696–699.
12. Alabi, A. A., M. I. Bahamonde, …, K. J. Swartz. 2007. Portability of paddle motif function and pharmacology in voltage sensors. *Nature*. 450:370–375.
13. Milescu, M., J. Vobecky, …, K. J. Swartz. 2007. Tarantula toxins interact with voltage sensors within lipid membranes. *J. Gen. Physiol.* 130:497–511.
14. Xu, Y., Y. Ramu, and Z. Lu. 2008. Removal of phospho-head groups of membrane lipids immobilizes voltage sensors of K^+ channels. *Nature*. 451:826–829.
15. Bosmans, F., M. F. Martin-Eauclaire, and K. J. Swartz. 2008. Deconstructing voltage sensor function and pharmacology in sodium channels. *Nature*. 456:202–208.
16. Banerjee, A., and R. MacKinnon. 2008. Inferred motions of the S3a helix during voltage-dependent K^+ channel gating. *J. Mol. Biol.* 381:569–580.
17. Milescu, M., F. Bosmans, …, K. J. Swartz. 2009. Interactions between lipids and voltage sensor paddles detected with tarantula toxins. *Nat. Struct. Mol. Biol.* 16:1080–1085.
18. Rogers, J. C., Y. Qu, …, W. A. Catterall. 1996. Molecular determinants of high affinity binding of α-scorpion toxin and sea anemone toxin in the S3-S4 extracellular loop in domain IV of the Na^+ channel α subunit. *J. Biol. Chem.* 271:15950–15962.
19. Swartz, K. J., and R. MacKinnon. 1997. Hanatoxin modifies the gating of a voltage-dependent K^+ channel through multiple binding sites. *Neuron*. 18:665–673.
20. Swartz, K. J., and R. MacKinnon. 1997. Mapping the receptor site for hanatoxin, a gating modifier of voltage-dependent K^+ channels. *Neuron*. 18:675–682.
21. Cestèle, S., Y. Qu, …, W. A. Catterall. 1998. Voltage sensor-trapping: enhanced activation of sodium channels by β-scorpion toxin bound to the S3-S4 loop in domain II. *Neuron*. 21:919–931.
22. Li-Smerin, Y., and K. J. Swartz. 2000. Localization and molecular determinants of the Hanatoxin receptors on the voltage-sensing domains of a K^+ channel. *J. Gen. Physiol.* 115:673–684.
23. Cestèle, S., and W. A. Catterall. 2000. Molecular mechanisms of neurotoxin action on voltage-gated sodium channels. *Biochimie*. 82:883–892.
24. Li-Smerin, Y., and K. J. Swartz. 2001. Helical structure of the COOH terminus of S3 and its contribution to the gating modifier toxin receptor in voltage-gated ion channels. *J. Gen. Physiol.* 117:205–218.
25. Lee, H. C., J. M. Wang, and K. J. Swartz. 2003. Interaction between extracellular Hanatoxin and the resting conformation of the voltage-sensor paddle in Kv channels. *Neuron*. 40:527–536.
26. Phillips, L. R., M. Milescu, …, K. J. Swartz. 2005. Voltage-sensor activation with a tarantula toxin as cargo. *Nature*. 436:857–860.
27. Lee, S. Y., and R. MacKinnon. 2004. A membrane-access mechanism of ion channel inhibition by voltage sensor toxins from spider venom. *Nature*. 430:232–235.
28. Suchyna, T. M., S. E. Tape, …, P. A. Gottlieb. 2004. Bilayer-dependent inhibition of mechanosensitive channels by neuroactive peptide enantiomers. *Nature*. 430:235–240.
29. Jung, H. J., J. Y. Lee, …, J. I. Kim. 2005. Solution structure and lipid membrane partitioning of VSTx1, an inhibitor of the KvAP potassium channel. *Biochemistry*. 44:6015–6023.
30. Smith, J. J., S. Alphy, …, K. M. Blumenthal. 2005. Differential phospholipid binding by site 3 and site 4 toxins. Implications for structural variability between voltage-sensitive sodium channel domains. *J. Biol. Chem.* 280:11127–11133.
31. Schmidt, D., and R. MacKinnon. 2008. Voltage-dependent K^+ channel gating and voltage sensor toxin sensitivity depend on the mechanical state of the lipid membrane. *Proc. Natl. Acad. Sci. USA*. 105:19276–19281.

32. Takahashi, H., J. I. Kim, …, I. Shimada. 2000. Solution structure of hanatoxin1, a gating modifier of voltage-dependent K^+ channels: common surface features of gating modifier toxins. *J. Mol. Biol.* 297:771–780.

33. Takeuchi, K., E. Park, …, I. Shimada. 2002. Solution structure of ω-grammotoxin SIA, a gating modifier of P/Q and N-type Ca^{2+} channel. *J. Mol. Biol.* 321:517–526.

34. Lee, C. W., S. Kim, …, J. I. Kim. 2004. Solution structure and functional characterization of SGTx1, a modifier of Kv2.1 channel gating. *Biochemistry.* 43:890–897.

35. Marvin, L., E. De, …, C. Lange. 1999. Isolation, amino acid sequence and functional assays of SGTx1. The first toxin purified from the venom of the spider *Scodra griseipes*. *Eur. J. Biochem.* 265:572–579.

36. Wang, J. M., S. H. Roh, …, K. J. Swartz. 2004. Molecular surface of tarantula toxins interacting with voltage sensors in K(v) channels. *J. Gen. Physiol.* 123:455–467.

37. Takahashi, H., T. Nakanishi, …, I. Shimada. 2000. A novel NMR method for determining the interfaces of large protein-protein complexes. *Nat. Struct. Biol.* 7:220–223.

38. Nakanishi, T., M. Miyazawa, …, I. Shimada. 2002. Determination of the interface of a large protein complex by transferred cross-saturation measurements. *J. Mol. Biol.* 318:245–249.

39. Takeuchi, K., H. Takahashi, …, I. Shimada. 2004. Channel-forming membrane permeabilization by an antibacterial protein, sapecin: determination of membrane-buried and oligomerization surfaces by NMR. *J. Biol. Chem.* 279:4981–4987.

40. Ladokhin, A. S., S. Jayasinghe, and S. H. White. 2000. How to measure and analyze tryptophan fluorescence in membranes properly, and why bother? *Anal. Biochem.* 285:235–245.

41. Ladokhin, A. S. 1997. Distribution analysis of depth-dependent fluorescence quenching in membranes: a practical guide. *Methods Enzymol.* 278:462–473.

42. Ladokhin, A. S. 1999. Analysis of protein and peptide penetration into membranes by depth-dependent fluorescence quenching: theoretical considerations. *Biophys. J.* 76:946–955.

43. Abrams, F. S., and E. London. 1992. Calibration of the parallax fluorescence quenching method for determination of membrane penetration depth: refinement and comparison of quenching by spin-labeled and brominated lipids. *Biochemistry.* 31:5312–5322.

44. Abrams, F. S., and E. London. 1993. Extension of the parallax analysis of membrane penetration depth to the polar region of model membranes: use of fluorescence quenching by a spin-label attached to the phospholipid polar headgroup. *Biochemistry.* 32:10826–10831.

45. Sean Peacock, R., A. M. Weljie, …, H. J. Vogel. 2005. The solution structure of the C-terminal domain of TonB and interaction studies with TonB box peptides. *J. Mol. Biol.* 345:1185–1197.

46. Weljie, A. M., and H. J. Vogel. 2004. Unexpected structure of the Ca^{2+}-regulatory region from soybean calcium-dependent protein kinase-α. *J. Biol. Chem.* 279:35494–35502.

47. Goddard, T. D., and D. G. Kneller. 2004. SPARKY 3. University of California, San Francisco, San Francisco, CA.

48. Wuttke, D. S., M. P. Foster, …, P. E. Wright. 1997. Solution structure of the first three zinc fingers of TFIIIA bound to the cognate DNA sequence: determinants of affinity and sequence specificity. *J. Mol. Biol.* 273:183–206.

49. Foster, M. P., D. S. Wuttke, …, P. E. Wright. 1997. Domain packing and dynamics in the DNA complex of the N-terminal zinc fingers of TFIIIA. *Nat. Struct. Biol.* 4:605–608.

50. Jayalakshmi, V., and N. R. Krishna. 2002. Complete relaxation and conformational exchange matrix (CORCEMA) analysis of intermolecular saturation transfer effects in reversibly forming ligand-receptor complexes. *J. Magn. Reson.* 155:106–118.

51. Wee, C. L., D. Bemporad, …, M. S. Sansom. 2007. SGTx1, a Kv channel gating-modifier toxin, binds to the interfacial region of lipid bilayers. *Biophys. J.* 92:L07–L09.

52. Nguyen, T. P., and R. Horn. 2002. Movement and crevices around a sodium channel S3 segment. *J. Gen. Physiol.* 120:419–436.

53. Gandhi, C. S., E. Clark, …, E. Y. Isacoff. 2003. The orientation and molecular movement of a K^+ channel voltage-sensing domain. *Neuron.* 40:515–525.

54. Darman, R. B., A. A. Ivy, …, R. O. Blaustein. 2006. Constraints on voltage sensor movement in the *shaker* K^+ channel. *J. Gen. Physiol.* 128:687–699.

55. Oswald, R. E., T. M. Suchyna, …, F. Sachs. 2002. Solution structure of peptide toxins that block mechanosensitive ion channels. *J. Biol. Chem.* 277:34443–34450.

56. Suchyna, T. M., J. H. Johnson, …, F. Sachs. 2000. Identification of a peptide toxin from *Grammostola spatulata* spider venom that blocks cation-selective stretch-activated channels. *J. Gen. Physiol.* 115: 583–598.